Valence- and conduction-band structure of the sapphire ($1\bar{1}02$) surface

W. J. Gignac* and R. Stanley Williams
Department of Chemistry and Biochemistry, University of California Los Angeles, Los Angeles, California 90024

Steven P. Kowalczyk
Rockwell International Corporation, Microelectronics Research and Development Center, Thousand Oaks, California 91360

(Received 16 July 1984)

X-ray photoelectron (XPS) and electron-energy-loss spectroscopies have been employed to investigate the valence- and conduction-band densities of states of the sapphire ($1\bar{1}02$) surface. The photoemission spectrum of the valence-band region has been adjusted to remove cross-section effects and compared to the recent theoretical density of states calculated by Ciraci and Batra. The energy-loss data have been used to determine the bulk-plasmon energy of sapphire, 24.0 ± 0.3 eV, as well as the locations of eight regions of high conduction-band—state density within 20 eV above the conduction-band minimum. One of these regions is an empty surface state 4.0 eV below the conduction-band minimum. Several high-binding-energy satellites in the XPS core-level spectra are reported and interpreted in terms of energy losses to plasmons and interband transitions.

I. INTRODUCTION

Aluminum oxide, Al_2O_3, in its various phases is important in a number of technological applications that include heterogeneous catalysts and microelectronic devices. In order to better appreciate the role of Al_2O_3 in these areas, a detailed understanding of the surface electronic structure of the different forms of Al_2O_3 is required. Previous experimental studies of Al_2O_3 used techniques such as optical-absorption and reflection spectroscopies,[1–3] electron-energy-loss spectroscopy (EELS),[4–6] and photoconductivity[7] to determine the bulk electronic structure of Al_2O_3. These electronic-structure studies were performed on samples ranging from single and polycrystalline α- and γ-Al_2O_3 to amorphous films. The main objective of the optical experiments was the determination of the band gap in the various forms of Al_2O_3. This determination was complicated by the possibility that an excitonic state existed near the conduction-band minimum (CBM).[3,8] In addition to the band-gap information, the absorption data of Arakawa and Williams[3] contained some intriguing features between 10 and 20 eV that could not be attributed either to plasmons or to excitonic transitions. Earlier EELS data by Swanson[5] contained features in the same energy regime that are apparently the result of interband transitions in Al_2O_3.

Several theoretical determinations of the electronic structure of various Al_2O_3 analogs have been performed. These calculations were based on semiquantitative models[9,10] or molecular units of the types AlO_4^{5-},[11] AlO_6^{-9},[12,21] and Al_2O_3.[13] More sophisticated calculations used semiempirical techniques, such as the Mulliken-Rudenberg method,[14] or the extended tight-binding approximation.[15] The most recent calculation, which employed a modified extended Hückel theory, is that of Ciraci and Batra,[16] who presented comparisons with good agreement between their theory and existing experimental data. They also presented the results of a calculation for a thin Al_2O_3 slab, which emphasized the surface contributions to the electronic structure.

The first attempt to establish the experimental Al_2O_3 band structure in the conduction, valence, and core regions was made by Balzarotti and Bianconi (BB).[17] They used x-ray photoelectron spectroscopy (XPS) on various forms of Al_2O_3, in conjunction with existing optical[3] and EELS data,[5] in order to establish the band structures of α-, γ-, and amorphous Al_2O_3. BB concluded that all three forms of Al_2O_3 had similar electronic structures. Especially noteworthy features were a core excitonic state just below, and a high density of states just above, the CBM. XPS data for α-Al_2O_3, which differed slightly from that of BB, were also reported by Kowalczyk *et al.*[18] The electronic structure of Al_2O_3 was also studied by x-ray-absorption spectroscopy (XAS),[19–24] x-ray-emission spectroscopy (XES),[23–26] and reflection EELS.[4,27,28] Reflection EELS can be performed with low-energy electron beams to enhance the sensitivity to surface losses. The EELS experiments of Olivier and Poirier[28] (OP) contained features which were not observed in previous optical measurements. Extensive studies of oxygen chemisorbed on well-defined Al surfaces have also been undertaken.[29] The x-ray-absorption results from some of these studies have been extrapolated to Al_2O_3 surfaces.[30,31] However, these experiments were performed on samples grown from the *in situ* oxidation of aluminum metal, the pyrolitic decomposition of $AlCl_3$, or amorphous Al_2O_3 samples which were sintered in air. Consequently, the phase composition of the samples in these studies was uncertain. In order to determine the bulk and surface electronic structure of the various phases of Al_2O_3, experiments should be performed on well-characterized surfaces of single crystals.

The most well-defined Al_2O_3 surfaces currently available are prepared from industrial sapphire (corundum), which is undoped, single-crystal α-Al_2O_3.[32] High-quality sapphire samples are commercially available, since several

different crystal faces are often used as substrates for epitaxial growth of silicon-on-sapphire (SOS) structures. The sapphire ($1\bar{1}02$) surface has been studied extensively by low-energy-electron diffraction (LEED), Auger-electron spectroscopy (AES),[33–35] and Rutherford backscattering spectroscopy[36] in conjunction with SOS applications.

In order to initiate more careful studies of the electronic structure of the various forms of Al_2O_3, this study employed a combination of XPS and reflection EELS techniques to gather information from a single crystal of sapphire oriented to expose a ($1\bar{1}02$) plane. The details of the experimental procedure used are discussed in Sec. II, and the results of the experiments are presented in Sec. III. The data are compared to the band-structure calculations of Ciraci and Batra[16] in Sec. IV, along with a discussion of how the interpretation of the present results compares and contrasts with the work of other investigators. The primary conclusions of this study are listed in Sec. V.

II. EXPERIMENTAL PROCEDURE

Single crystals of sapphire oriented and polished on the ($1\bar{1}02$) plane were obtained from the Union Carbide Company, Crystal Products Division. Using a diamond-tipped scribe, samples were cut to approximately 5×15 mm^2 for the EELS studies and 5×5 mm^2 for the XPS experiments.

A. XPS measurements

The XPS measurements were performed with an ultrahigh-vacuum- (UHV) modified Hewlett-Packard 5950A electron spectrometer equipped with a monochromatized Al $K\alpha$ ($h\nu=1486.6$ eV) x-ray source. The spectrometer resolution was 0.6 eV full width at half maximum (FWHM), and spectra were collected with a photoelectron emission angle 51.5° from the sample normal. The Al_2O_3 crystal used for the XPS experiments was etched in HF for 2 min, rinsed in H_2O, blown dry with N_2, and mounted on a molybdenum plate with indium. The sample was then immediately loaded into the spectrometer vacuum system. The sample was heated in UHV (5×10^{-9} Torr) for several minutes at 750°C. This procedure produced a clean Al_2O_3 surface as determined by an XPS survey scan [(0—1000)-eV binding-energy region]. The only observed contamination was F (approximately $\frac{1}{100}$ monolayer) residue from the chemical-etch treatment. No LEED pattern was observed from this surface. High-resolution spectra of the Al $2s$, Al $2p$, and O $1s$ core levels, as well as the O KVV Auger transition and the valence-band region were obtained. Al and O appeared to be in only one chemical state. No growth of O or C during the course of the measurements was observed by monitoring the O $1s$ and C $1s$ regions before and after the measurements.

B. EELS and AES measurements

Prior to the EELS and AES experiments, the samples were ultrasonically cleaned in acetone and methanol and then dipped in a concentrated solution of HF for 30 sec. Sample heating was accomplished by a method similar to that of Chang.[33] In this study, a sandwich was made by placing a 0.02-mm Ta sheet between two sapphire crystals and the set was securely tied together with two Ta wires. The sandwich was mounted by clamping excess Ta sheet, which extended from both ends of the sandwich, to the sample manipulator (Varian model 981-2523). The sample was heated by passing a current of up to 10 A through the Ta sheet. Approximate sample temperatures were measured by means of a Pt—Pt/10% Rh thermocouple that was spot-welded to the Ta heater near the sapphire crystals. An optical pyrometer was used for the highest temperature range. Once under vacuum, the samples were cleaned by successive Ar^+-ion bombardment (typically 1.5 kV at 20 mA) and heating to approximately 1500°C. After the initial cleaning cycle, the samples were recleaned every day by heating only.

The EELS experiments were conducted in an ion-pumped UHV chamber with a typical base pressure of 2×10^{-10} Torr. The chamber was equipped with a standard Varian LEED system which was used to determine the two-dimensional order of the sample surface. AES and EELS were performed with a PHI single-pass cylindrical mirror analyzer (CMA) and coaxial electron gun (PHI model 10-234G). The sample was always oriented perpendicular to the incident electron beam. For AES the instrument was run in the $dN(E)/dE$ mode, while the $-d^2N(E)/dE^2$ mode was used for EELS.[37–39] A DEC LSI 11/23 minicomputer controlled the pass energy of the CMA. This computer control allowed accurate data collection over long counting times, precise assignment of loss energies with respect to the incident electron energy, and the ability to numerically integrate the differentiated spectra that result from phase-sensitive detection. An EELS sweep over 25 eV required from 5 to 30 min depending on the proximity of the sweep to the incident beam energy and the kinetic energy of the collected electrons. For a 150-eV incident electron beam, an effective modulation voltage of 1 V peak-to-peak resulted in an elastic peak with a 1 eV FWHM.

III. RESULTS

A. XPS: The valence and core states

The XPS valence-band spectrum of ($1\bar{1}02$) sapphire is shown as the top curve in Fig. 1. Because of charging problems inherent in insulators, XPS data are commonly referenced to the valence-band maximum (VBM) or, if accurate optical data are available, to the CBM. In this paper, all XPS data are referenced to the CBM, which is defined as the experimentally determined VBM plus the optical band gap of 8.5 eV, as suggested by Oliver and Poirier (OP).[28] The valence-band region is separated into two distinct bands, which will be called the upper valence band (UVB) and the lower valence band (LVB) after Ciraci and Batra.[16] The energy of the UVB maximum is determined from the XPS data by joining an extrapolation to the region of steepest descent in the valence-band electron-distribution curve with a linear extrapolation of the baseline. The same procedure is used for the UVB minimum, except that the region of steepest descent is re-

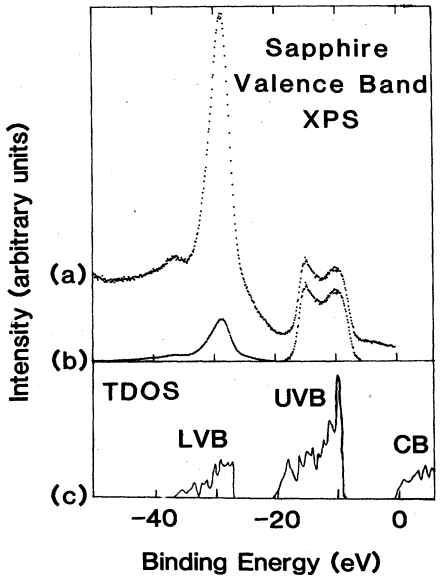

FIG. 1. (a) Valence-band XPS data for $(1\bar{1}02)$ sapphire obtained with monochromatized Al $K\alpha$ x radiation. All XPS spectra presented in this paper are referenced to the conduction-band minimum. (b) XPS data shown in (a) after background subtraction and scaling in order to reduce the area under the LVB by a factor of 7.3 with respect to the area under the UVB, in accordance with the calculated photoionization cross sections for O $2s$ and O $2p$ subshells (Ref. 40). (c) The theoretical total density of states for sapphire from a band-structure calculation by Ciraci and Batra (Ref. 16).

placed by the region of steepest ascent. In this way, the width of the UVB is determined to be 9.7 eV. This method has been used previously for insulators[18] and gives good agreement with other methods.[17] The LVB region contains two intensity maxima, a major peak at 28.8 eV and a minor peak at 35.5 eV with respect to the CBM. Because of the high sloping background, it is not possible to determine the positions of the energy minimum or

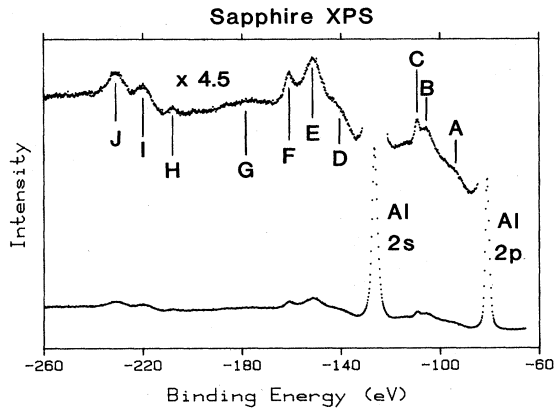

FIG. 2. XPS data for sapphire in the energy region near the Al $2p$ and $2s$ core levels. The lower curve shows the Al $2p$ and $2s$ core lines and the background on the same scale. The upper curve is an enlargement of the background and clearly shows XPS satellites which are labeled A through J.

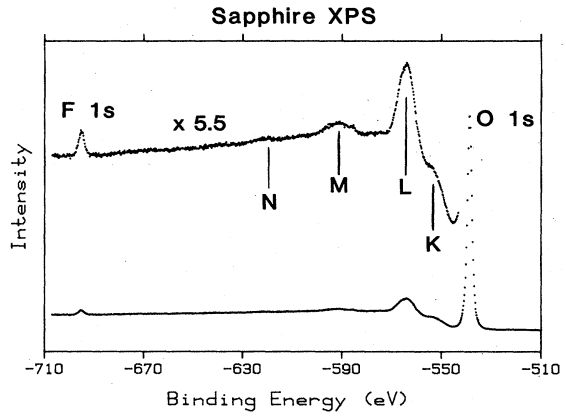

FIG. 3. XPS data for sapphire including the O $1s$ and F $1s$ core lines. Fluorine is the only impurity detected by XPS. The upper trace is an enlargement of the energy range behind the O $1s$ line and contains satellites labeled K through N.

maximum of the LBV very precisely, but the width of the LVB must be somewhat larger than the separation between the two peaks, 6.7 eV.

All of the accessible core lines, the Al $2p$, Al $2s$, and O $1s$ that are seen in Figs. 2 and 3, apparently consist of single lines and are assigned energies that correspond to the peak maxima. The energies for all of the observed occupied states are contained in Table I, along with values extracted from the XPS data of BB,[17] with the present definition of the VBM. Examination of the XPS data in the regions behind the LVB, Al $2p$, Al $2s$, and O $1s$ core lines, reveals a large number of satellites on the high binding energy side of the core lines. These satellites are labeled A through N in Figs. 2 and 3. Only one broad satellite is observed for the LVB. This satellite occurs ap-

TABLE I. XPS binding energies in sapphire and MgO.

XPS feature	Sapphire This work (eV)[a]	Sapphire Ref. 17 (eV)[a]	MgO Refs. 18 and 41 (eV)[a]
Upper valence band			
Energy maximum	8.5±0.3	8.5±0.3	7.5±0.3
Peak 1	11.8	11.8	10.0
Peak 2	16.5	15.8	12.7
Energy maximum	18.2		14.0
Lower valence band			
Major peak	28.8	29.3	26.3
Minor peak	35.5		30.0
Mg $2p$			54.5
Mg $2s$			92.9
Al $2p$	80.9	79.9	
Al $2s$	126.0	124.9	
O $1s$	538.6	537.0	

[a]All energies are referenced to the respective conduction-band minima. Band gaps of 8.5 eV (Ref. 28) and 7.5 eV (Ref. 54) are assumed for sapphire and MgO, respectively.

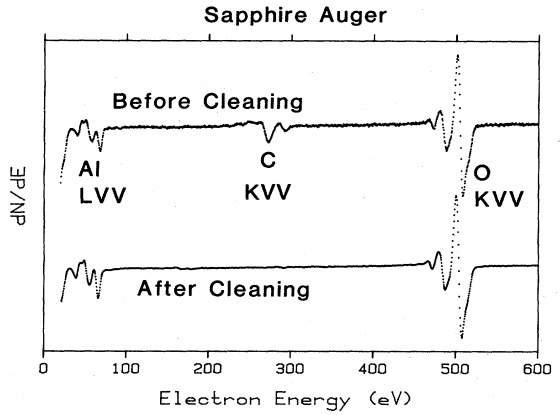

FIG. 4. Representative AES for $(1\bar{1}02)$ sapphire. The upper curve was taken before the sample was cleaned and contains a peak due to carbon contamination. The lower curve is typical for a clean sample. The spectral features of note are the minima between 35 and 70 eV due to Al *LVV* processes and those near 512 eV from O *KVV* processes. Except for the carbon contamination, the spectra are identical before and after cleaning, and no changes were observed from the clean spectra with electron bombardment during these experiments.

proximately 25 eV higher in binding energy than the major LVB feature at 28.8 eV.

B. LEED and AES

Prior to the EELS experiments, the order and composition of the $(1\bar{1}02)$ sapphire surface was examined by LEED and AES. The AES data, shown in Fig. 4, were taken before any in-vacuum sample processing and after the sample was cleaned by Ar^+ bombardment and annealing. The Al *LVV* region of the AES data consists of three features at 35, 53, and 67 eV, while the signal due to O *KVV* Auger electrons is observed around 512 eV. Two features near 280 eV due to carbon, and perhaps also to calcium, contamination are also seen in the spectrum taken before cleaning. The spectrum taken after the sample was cleaned is representative of the sample surface both before and after EELS data were collected. The AES spectrum of clean sapphire is very similar to that of sapphire before cleaning with the exception of the impurity peaks, which are absent from the clean surface. The observation that the Al *LVV* portion of the spectra does not change during the course of the EELS experiments indicates that the surface is not significantly damaged by the electron beam.

The LEED pattern of the clean and annealed sapphire surface revealed a 2×1 reconstruction of the nearly fourfold-symmetric $(1\bar{1}02)$ plane, which was previously observed by Chang.[34] The LEED pattern consisted of fairly sharp spots at beam energies down to about 90 eV. Below 90 eV, however, the LEED spots started to become diffuse and often faded away entirely after several minutes. The LEED and AES investigations showed that the surface was extremely clean, chemically stable, and well ordered throughout the EELS data collection.

C. EELS: The conduction-band states and the bulk plasmon

EELS data were collected for $(1\bar{1}02)$ sapphire in five significant energy-loss regions, which should correspond to the excitation of transitions from the various initial states to the conduction band. Losses in the EELS spectra may also rise from the excitation of plasmons in the sample. The EELS spectra displayed in Figs. 5 through 9 correspond to possible interband transitions originating from the UVB, LVB, Al $2p$, Al $2s$, and O $1s$ states, respectively. There are 31 characteristic energy losses in these spectra that have been labeled (a) through (ee). Although some of the energy-loss features in the spectra appear to be weak, they were all very reproducible from day to day and from sample to sample. EELS spectra were collected at several different incident-electron-beam energies for each loss region, and spectra were also collected after varying amounts of electron-beam dose to a particular spot on a sample. No variations occurred in the EELS spectra that could be attributed to electron-beam damage to the samples, and the EELS spectra appeared to be unaffected by sample charging for incident beam energies of 150 eV or higher.

After the EELS experiments on clean sapphire were completed, nickel was evaporated onto the sapphire in amounts ranging from 0.5 to 5 equivalent monolayers, as

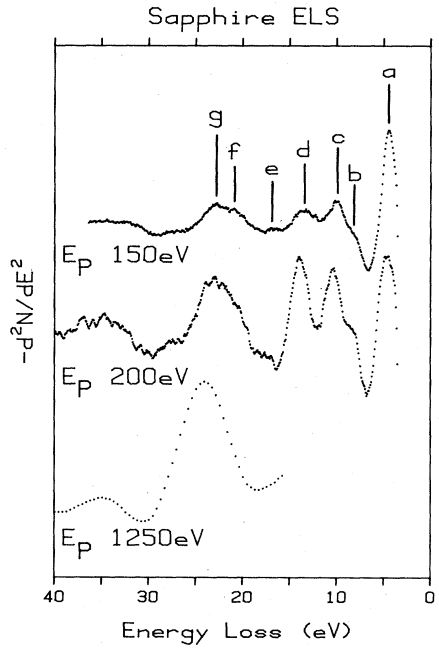

FIG. 5. Negative second-derivative energy-loss spectra, $-d^2N/dE^2$, as a function of loss energy for $(1\bar{1}02)$ sapphire. Peaks in this energy range must be due to plasmon losses or interband transitions between the valence and conduction bands. Spectra are shown for three different incident beam energies (E_p) to demonstrate the loss-feature-intensity dependence on electron kinetic energy. Features are labeled (a) through (g). Note that feature (a) occurs at less than 5 eV, well below the sapphire band gap.

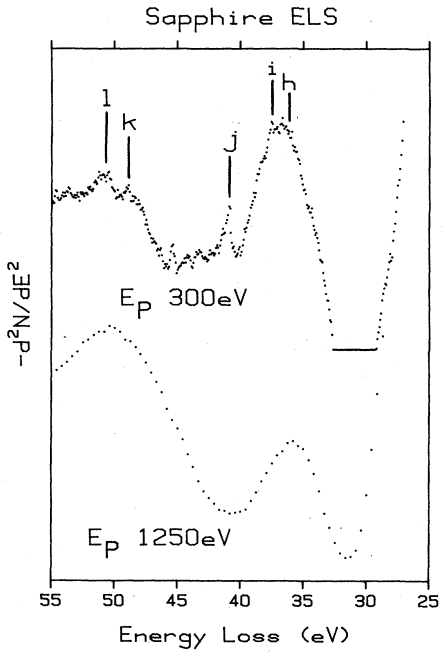

FIG. 6. Energy-loss spectra for interband transitions with O 2*s* or lower valence-band initial states in sapphire. Features are labeled (h) through (l) and the energy position near feature (k) is the expected location of a double plasmon loss.

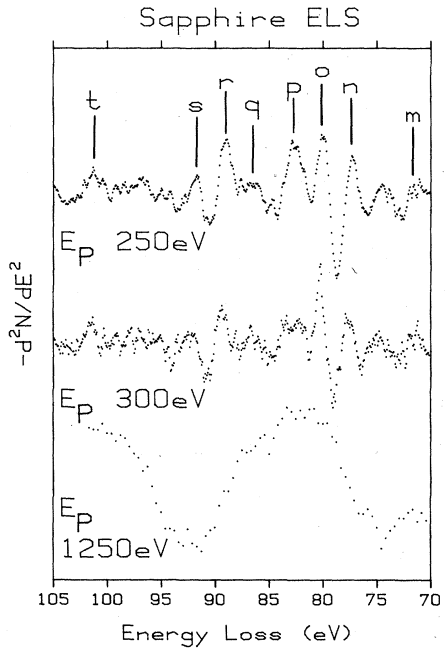

FIG. 7. Energy-loss spectra for interband transitions with Al 2*p* initial states in sapphire. Incident beam energies of 250 and 300 eV show sharp features [(m) through (t)], while the features are smoothed out in the 1250-eV spectrum because of the poor resolution of the CMA at high electron kinetic energies. Feature (m) is the energy location expected for a triple bulk-plasmon loss.

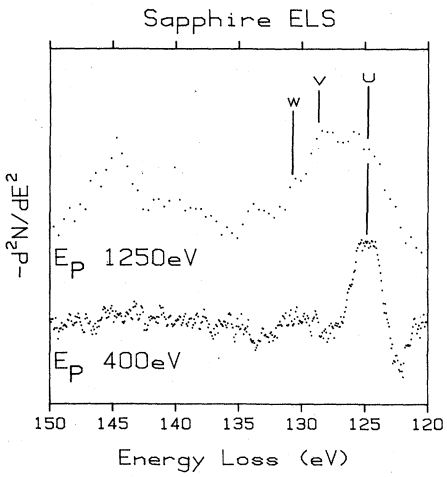

FIG. 8. Energy-loss spectra for interband transitions with Al 2*s* initial states. The incident-electron-beam energies shown are 400 and 1250 eV. Although the features labeled (u) and (w) are weak, they appeared reproducibly in several different spectra at 1250 eV.

monitored by a quartz-crystal microbalance. In all cases, the addition of nickel resulted in severe surface charging, which did not allow a LEED pattern to be observed below incident beam energies of approximately 200 eV. The AES data also showed significant distortion from 0 to 200 eV. Analysis of the AES signal intensities versus the amount of nickel deposited indicated that the nickel formed islands on the surface and did not cover the entire surface even when present in amounts equivalent to 5 monolayers. This experiment showed that metal impurities on the sapphire surface may act as charge traps, and that the surface must be extremely clean before meaningful results may be obtained with electron spectroscopic techniques.

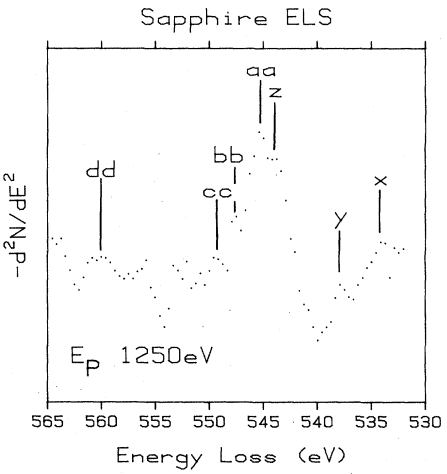

FIG. 9. Energy-loss spectra for interband transitions with O 1*s* initial states. Low intensities at low incident beam energies forced the use of a 1250-eV incident-beam-energy spectrum where the CMS resolution is low. However, all the labeled features were reproducible.

D. XPS satellites

A close examination of the XPS data displayed in Figs. 2 and 3 reveals several high-binding-energy satellites associated with each core level. It is very likely that these satellites are related to the energy losses observed in the EELS spectra. Figures 10 and 11 have been constructed to show the relationship between the XPS satellites and EELS data. The EELS data, originally displayed in Figs. 5–9, are displayed as a function of $N(E)$, rather than of $-d^2N/dE^2$. This numerical double integration is possible because the data were collected digitally. Because of the complexity of Figs. 10 and 11, all features are referenced to the labels in Figs. 2 and 3. In Fig. 10, the O 1s XPS data are plotted with the O 1s core line as the zero of energy. From this point of view, all of the features in the electron-distribution curve are a consequence of O 1s photoelectrons which lose energy. Figure 11 is similar to Fig. 10, except that the satellites from both Al 2p and Al 2s photoelectrons are seen together. The upper energy scale and EELS data use Al 2s as the energy zero, while the lower-energy scale and EELS are referenced to Al 2p.

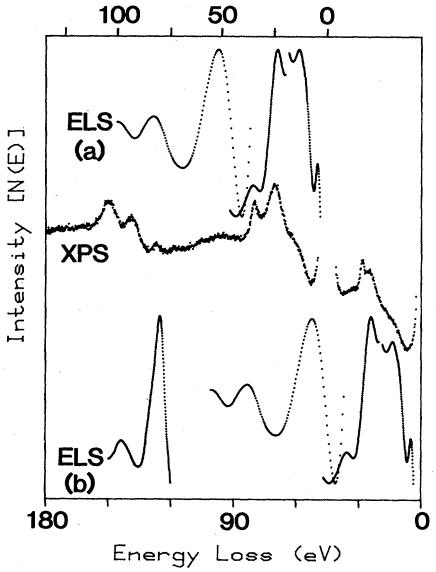

FIG. 11. The three parts of this figure allow the Al 2p and 2s satellites to be compared with EELS data. XPS: The XPS data in the Al 2p and 2s regions are enlarged and plotted with the maximum of the Al 2p line as the zero of energy on the bottom scale and the Al 2s line as the zero of energy on the top scale. ELS: (a) These curves are integrated energy-loss spectra, similar to Fig. 10, plotted with the Al 2s line as the zero of energy loss. (b) Integrated energy-loss spectra plotted with the Al 2p line as the zero of energy loss.

IV. DISCUSSION

A. XPS: Valence-band density of states

The XPS data were collected to obtain an accurate picture of the valence and core density of states (DOS) in sapphire. The raw XPS valence-band data of Fig. 1(a) and the theoretical DOS shown in Fig. 1(c), which was taken from the work of Ciraci and Batra,[16] are in qualitative agreement in that both have significant intensity in the same energy regions. The calculation has not been adjusted to agree with the experiment. However, there is a large difference between experimental and theoretical intensity ratios of the UVB to the LVB.

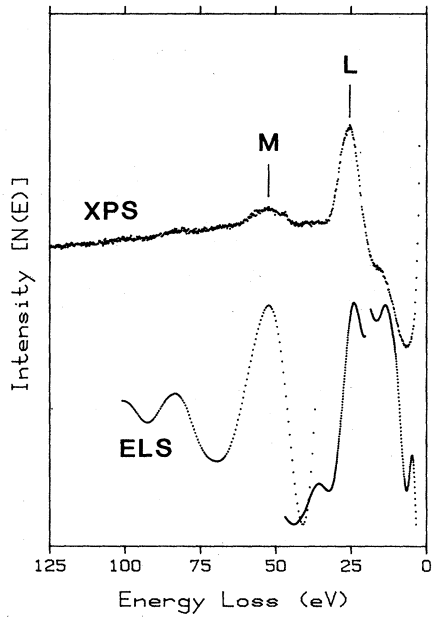

FIG. 10. Comparison of the XPS satellites to the EELS data. XPS: The XPS data for the O 1s core line plotted with the maximum of the O 1s line as the zero of energy. This emphasizes the assignment of XPS satellites as energy losses from O 1s photoelectrons. EELS: $N(E)$ electron-energy-loss spectra, versus loss energy, for sapphire. Selected doubly differentiated loss spectra from Figs. 5 through 9 were numerically integrated and plotted as $N(E)$ versus energy loss.

This discrepancy may be partly resolved if photoionization cross-section differences for the initial states of different orbital symmetry are considered. In order to obtain some quantitative correction to the ratio of the experimental UVB to LVB DOS, the cross sections for the sapphire valence band were approximated by the cross sections for free O^{2-} subshells. The band-structure calculations[16] show that UVB and LVB are primarily O 2p and 2s in character, respectively. The Hartree-Slater calculations of Scofield[40] yield a ratio of 7.3 for the photoionization cross sections of O 2s to O 2P for Al $K\alpha$ excitation. The curve shown in Fig. 1(b) is the valence-band XPS spectrum after an arbitrary background has been subtracted and the integrated intensity of the LVB has been lowered by a factor of 7.3 with respect to the UVB. The resulting agreement between the ratio of the intensity under the UVB to that under the LVB between the modified experimental DOS and the theoretical band structure demonstrated in Fig. 1 is quite good. Further examination of the modified XPS data reveal that the ratio of the UVB to LVB DOS is approximately 2.5 to 1. If O^{2-} were a perfect model for the sapphire valence band, this ratio

would be exactly 3 to 1. This level of agreement demonstrates that the corrected XPS data are reasonably self-consistent. The major discrepancy between Figs. 1(b) and 1(c) is the relative intensity of the different features within the UVB, where the XPS data show two main features of nearly equal intensity, but the calculation contains one dominant peak with several smaller ones. This difference may be caused in part by the resolution function of the photoelectron spectrometer and by variations of the photoemission cross section within the valence bands, which do contain some Al character according to Ciraci's and Batra's calculations.[16]

The XPS data presented in Figs. 1–3 and those of BB (Ref. 17) are in general agreement, as demonstrated by Table I, but there are a few discrepancies between the two sets of data. Figure 1 of BB shows three distinct features in the UVB region, while Fig. 1(a) provides no evidence of their highest-binding-energy feature. Older data by Kowalczyk *et al.*,[18,41] on an Ar^+-bombarded surface, are also missing this third feature, which is most likely the result of residual carbon contamination. In addition, BB attribute the asymmetry of the LVB feature to an unresolved plasmon satellite about 23 eV below the VBM. However, Fig. 1(a) shows two clearly resolved peaks in the LVB region. The theoretical DOS from Ref. 16 in Fig. 1(c) shows a broad LVB and a reasonably high DOS at a binding energy that corresponds to the minor peak in the experimental LVB region. Thus, the minor peak in the LVB region of the XPS spectrum is caused by a transition from the appropriate initial state, rather than by an energy loss.

B. Sample quality and electron-beam damage

In their EELS study of polycrystalline thin-film α-Al_2O_3, OP (Ref. 28) suggested that exposure to the primary electron beam dissociated Al_2O_3 to produce either metallic Al or reduced oxides of the form AlO_x on the sample surface. As evidence for this process, they note the presence of a peak at 67 eV in the Al *LVV* Auger spectrum, which was attributed to metallic Al. However, the Al *LVV* region of the AES data of this study (Fig. 4) is exactly the same before and after the electron-beam exposures required to collect EELS spectra. Additional evidence for the possibility of Al_2O_3 surface modification as a result of extensive exposure to an electron beam is provided by the EELS spectra of Balzarotti *et al.*[21] Initially, the spectrum for clean α-Al_2O_3 (Fig. 2 of Ref. 21) is very similar to those shown in Fig. 5 of this study. However, after 90 min of exposure to a 300-eV electron beam of unspecified current, the EELS spectrum evolved until it resembled that of Al metal more than α-Al_2O_3. In the current study the EELS spectra do not change over a period of days or from sample to sample. Therefore, the electron beam is not damaging the sample in these experiments unless the damage is done during the first AES scan. The 67-eV AES feature in Fig. 4 could be the result of chemically different Al at or near the surface which is intrinsic to a clean sapphire $(1\bar{1}02)$ surface. Although the XPS data do not provide evidence for more than one chemically distinct Al species, electron mean free paths in sapphire indicate that the XPS sampling depth ranges from approximately 25 to 50 Å for O 1*s* and Al 2*s* and 2*p* photoelectrons, whereas Auger electrons of about 50 eV sample only about 5 Å into the crystal.[42] Therefore, a distinct Al surface species chemically shifted with respect to bulk Al may be seen by AES and not XPS. This may be seen clearly in the XPS spectra of Al metal with a thin oxide coating reported by Williams *et al.*[43] In the usual sample geometry of the HP5950A spectrometer, the chemically shifted Al 2*p* peak was not observable, but was clearly evident when the sample geometry was changed to grazing electron collection angles to enhance the surface sensitivity. It is also possible that the surface species identified by the Auger spectra was not present at all on the surfaces analyzed by XPS, since the samples were prepared by slightly different methods.

C. Sapphire plasmon

Using the simplest model for the volume plasma of an insulator,[44] the sapphire bulk-plasmon energy may be calculated to be 25.5 eV assuming that only electrons in the UVB contribute to the plasma. The number density of electrons is estimated to be 6 times the density of oxygen atoms (i.e., each O^{2-} ion contains six 2*p* electrons), and the band gap of sapphire is 8.5 eV. Previous studies of sapphire and anodized aluminum by optical reflectance and absorption (Refs. 2 and 3) and EELS (Refs. 4–6 and 28) place the volume plasmon energy anywhere from 22 to 26 eV. In this study, peaks *g*, *k*, and *m* in the EELS spectra occur at 24.0, 48.6, and 71.6 eV loss energy, respectively, and have been assigned to one, two, and three quanta losses to the bulk plasmon. A least-squares fit to these loss energies as a function of the number of quanta excited results in a volume plasmon energy of 24.0 ± 0.3 eV, in fair agreement with the above estimate. The present determination should represent a reasonably accurate value for the *q*-averaged plasmon energy, since it is based on essentially three independent observations.

D. Interband transitions and surface states

The energy-loss features that are not assigned to plasmon losses can be analyzed in terms of interband transitions. For a simple one-electron model, in which any relaxation effects in photoemission transitions or excitonic effects in interband transitions are neglected, the interband transitions can be described as electronic excitations from bound states, either valence or core, to an unoccupied state in the conduction band. The XPS data presented previously provide the energy position of the initial states. Consequently, the energy of final states can be determined in this one-electron approximation by adding the energy of a loss feature due to an interband transition to the appropriate initial-state energy. A set of one-electron final states for sapphire was determined by using the method described above with the XPS and EELS data for the LVB, Al 2*p*, Al 2*s*, and O 1*s*. Only EELS peaks which may be assigned to final states that were accessed from at least three different initial states are considered here. The final-state data, in conjunction with the energy loss data of Fig. 5, were then used to determine the initial

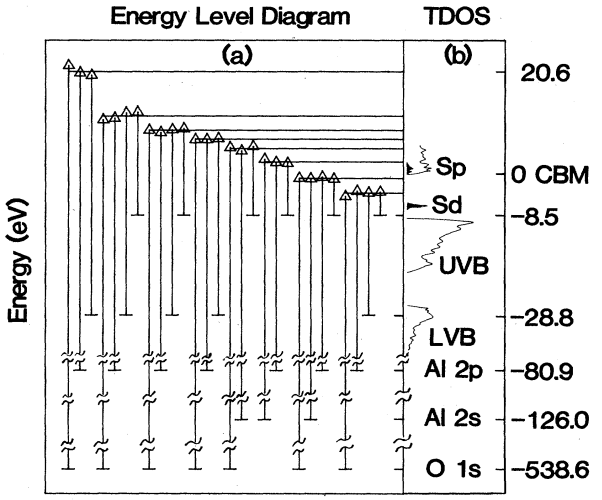

FIG. 12. (a) The empirical one-electron energy-level diagram for $(1\bar{1}02)$ sapphire. Occupied state energies were extracted from the XPS data, while the conduction-band energies were obtained by adding the loss energies from the EELS data to the initial-state energies. Conduction-band states are shown as horizontal lines. EELS transitions are represented by arrows from the initial to final states with the arrow heads (triangles) centered on the final-state energy. (b) A theoretical density of states from a band-structure calculation by Ciraci and Batra (Ref. 16) for a 16-layer slab of sapphire terminated at a (0001) surface. The percentage of Al character in the two band-gap states is represented by the black shading.

states of the transitions which originate in the UVB. This procedure was used because the XPS data in Fig. 1(a) show that the UVB's are very broad and do not have a single identifiable peak. The one-electron energy-level diagram, which is consistent with both the core-level and valence-band data, is shown in Fig. 12. The 28 labeled interband transitions terminate at eight well-defined final-state regions, which are listed in Table II. Assigning the UVB maximum and minimum as the two possible initial states for the lowest-energy-loss features gives the best agreement with the final states determined from the core initial-state energy-loss features. The spectra are collected not as $N(E)$ versus E, but as $-d^2N/dE^2$, so that the sharp step functions present at the LVB minimum and maximum can yield peaks in the EELS spectra if the final state of the transition is narrow.

Balzarotti *et al.*[21] have made soft-x-ray-absorption measurements on thin Al_2O_3 samples which were made by sintering amorphous films in air. These samples were identified as α-Al_2O_3 with a background of the γ phase. Features in the x-ray-absorption spectrum were assigned to electronic transitions between an Al $2p$ initial state and regions of the conduction band. Energies of high state density in the conduction band, which are consistent with the absorption spectrum (Fig. 3 of Ref. 21), are listed in the second column of Table II. In order to compare the EELS results from the current study with the x-ray-absorption data, a binding energy of 80.9 eV was assigned to the Al $2p$ level (Balzarotti *et al.* used a value of 79.98 eV). Also, the energy of the excitonic peak, as measured from Fig. 3 of Ref. 21, was taken to be 79.5 rather than 78.9 eV, as listed in Table I of that paper, and feature A_5 was located at 91.0 rather than 90.0 eV. The agreement between the absorption and EELS data, which can be seen in Table II, is fairly good at energies of less than 10 eV above the CBM. Over 10 eV, the x-ray-absorption data have a broad and intense absorption band that is not seen in the EELS.

The most intriguing part of the energy-level diagram (Fig. 12) is the state that occurs 4.0 eV below the CBM. Feature (a) at 4.7 eV loss energy in Fig. 5 provides the best evidence for this energy level. Because the minimum energy of the band gap in sapphire is 8.5 eV, the interband transition corresponding to this feature must have an initial state in the valence band and a final state at least 3.8 eV below the CBM. EELS transitions to this band-gap state were also reproducibly seen for Al $2p$ [feature (n)] and O $1s$ [feature (x)] initial states (see Figs. 7 and 9). The spectra in Fig. 5 show that the relative intensity of feature (a) decreases with respect to the other features as a function of increasing electron kinetic energy This behavior is exactly what would be expected if either the initial or final state of the interband transition were a surface state. Because core EELS transitions to the same final state also show this dependence, the band-gap state appears to be a surface state.

TABLE II. Conduction-band energy levels for sapphire and MgO. All energies are referenced to the conduction-band minimum. For sapphire and MgO, band gaps of 8.5 and 7.5 eV, respectively, were chosen.

Sapphire		MgO
EELS (eV)	X-ray absorption[a] (eV)	EELS[b] (eV)
−4.0±0.3		−3.2
−1.0±0.2	−1.4	−0.8
	1.1	1.5
2.3±0.3	2.1	3.3
5.0±0.4	4.3	3.5
6.9±0.1	7.3	6.4
8.7±0.3		11.4
	10.0	14.1
11.6±0.5		15.7
	15.0	18.7
	17.1	20.0
20.6±1.0	20.1	23.0

[a]Conduction-band energy levels calculated from the x-ray-absorption data of Balzarotti *et al.* (Ref. 21). To facilitate comparison of EELS and absorption data, a value of −80.9 eV was used for Al $2p$ binding energy rather than −79.98. All energies for features in the absorption spectrum were taken from Table I of Ref. 21, except for excitonic and A_5 features (assigned values of 79.5 and 91.0 eV, respectively), as measured from Fig. 3 of Ref. 21.

[b]Conduction-band values for MgO calculated from EELS data in Ref. 52 and XPS data in Refs. 18 and 41. No error estimates for the EELS data provided.

The EELS spectra for Al_2O_3 by Balzarotti *et al.*[21] have been discussed previously in regard to the surface modification by electron-beam irradiation. It is important to reiterate that the spectrum of the undamaged surface of polycrystalline α-Al_2O_3 is virtually identical to those shown in Fig. 5 and a feature at approximately 5 eV loss energy is observed by Balzarotti *et al.* which is similar to feature (a). This feature does not appear in the clean Al spectrum and does not change appreciably as the surface is reduced by electron-beam exposure. If the feature at 5 eV loss energy is associated with a surface state, then the existence of this feature in the EELS of a polycrystalline sample and its invariance during the reductive removal of O from the surface indicate that the surface state is likely to be derived from Al dangling-bond orbitals.

OP (Ref. 28) used the results of their EELS experiments in conjunction with the XPS data of BB, XAS and XES data of Brytov and Romashchenko, and the optical data of Arakawa and Williams[3] in a manner similar to that described above to determine a high density of conduction-band states at -1.0, 1.0, 5.1, 9.8, and 19.5 eV with respect to the CBM. These states are in reasonable agreement with the present results, but several points should be noted in comparing the results of the two experiments. First, OP looked at thin polycrystalline films instead of a single-crystal surface. Visual inspection of the EELS data presented in Figs. 2 through 4 of OP and that in Figs. 5 through 9 in this paper shows that the present spectra have significantly better resolution, and there is no reliable way to estimate the signal-to-noise ratio in the OP spectra because their figures appear to be hand-drawn representations of their data. In addition, OP reported three features at loss energies of 3.8, 4.2, and 5 eV, which they interpreted as indicating the presence of reduced Al produced by electron-beam irradiation on their samples (they also observed features at 3.6, 4, and 5.2 eV on metallic aluminum). No evidence for electron-beam reduction of the sapphire surface during EELS or AES measurements has been found in this study, but a great deal of care must be taken in assigning the low-energy EELS features that have been observed.

The ultraviolet-absorption spectra and spectrochemical analysis of sapphire crystals obtained from Union Carbide Corporation, similar to those used in our XPS and EELS experiments, have been reported by several groups.[45–47] These sapphire samples were found to contain less than 5 ppm each of common transition-metal impurities including Fe, Ni, Cr, Co, Mn, V, and Ti, each of which has been found to produce absorption bands between 3 and 8 eV in sapphire.[48] In addition, the absorption spectra from as-received samples were essentially flat between 3 and 8 eV. However, exposure of such samples to high-energy particle beams of neutrons or electrons,[45–47,49,50] or heating to 2000 °C in a reducing atmosphere for 2 h,[46,51] resulted in the appearance of several absorption bands between 4.8 and 6.5 eV and one emission band at 3.8 eV. These bands are caused by the formation of F^+ and F centers, oxygen vacancies in the crystal that are filled by one or two electrons. An alternative explanation for the low-energy EELS features observed by OP is that in generating their Al_2O_3 sample from the pyrolitic decomposition of $AlCl_3$ in a CO and H_2 atmosphere, a large number of defects were also formed in the crystallites. A set of experiments on Al_2O_3 samples grown under similar conditions to those employed by OP have found a series of trap states between 2.7 and 3.9 eV below the CBM,[52] which would account for the EELS features observed by OP.

The studies in which color centers were induced in sapphire by reduction heating or high-energy particle bombardment indicate that the sapphire crystals used in this study were free of defects induced by sample preparation. The Auger and EELS data indicate that the sapphire was not damaged by electron irradiation unless extremely low beam doses permit the reduction and removal of O. The temperature used to anneal the sample also was not high enough, nor was it sustained long enough to create many O vacancies, since temperatures near 1800 °C for 2 h in a reducing atmosphere did not create absorption bands in sapphire.[51] Consequently, the energy level 4 eV below the CBM is almost certainly an intrinsic surface state of sapphire ($1\bar{1}02$). The relative intensity of both the shoulder labeled (b) in Fig. 5 and the -4-eV surface state decreases with respect to the remaining spectral features upon oxygen exposure. Since feature (b) is associated with a transition that has an energy 1 eV below the CBM as a final state, this level may also be a surface state, although this energy region is also where the bulk exciton is found.

The results of a band-structure calculation by Ciraci and Batra[16] for a slab of sapphire oriented along an Al-terminated, unreconstructed (0001) face are shown in Fig. 12(b). This calculation yields two empty band-gap states, labeled S_p and S_d, which are approximately 1 and 5.3 eV below the CBM, respectively. Both of these states are derived mainly from surface-layer Al broken-bond orbitals. Although the calculations were performed for a (0001) plane of sapphire and the experiments were performed on a ($1\bar{1}02$) surface, the correspondence between theory and experiment suggests that both the experimentally observed band-gap states are surface states due to an Al-terminated ($1\bar{1}02$) sapphire surface. The presence of Al with broken bonds at the surface was also suggested by the Auger spectra of Fig. 4, which indicated that the sample has two chemically different Al species near the surface. Soft-x-ray-absorption experiments of oxygen chemisorbed on Al single crystals suggest that the chemisorbed systems have two surface states approximately 2.5 and 3.5 eV below the excitonic feature.[30,31] However, because potentially large differences exist between the chemisorbed system and bulk α-Al_2O_3, as seen near the absorption threshold in Fig. 1 of Ref. 31, it is not possible to relate these features to the -4.0-eV surface state determined in the current study.

The surface state 4 eV below the CBM may be invoked to explain the relatively small amount of charging observed on clean sapphire surfaces. Because the surface state is delocalized over the crystal surface, it may enable electrons impinging on the sample to flow rapidly away from the point of beam impact. However, impurities on the surface, such as nickel, may form localized trap states on the surface which could cause the large charging effects reported in the preceding section.

All of the one-electron transitions in the EELS spectra

of sapphire have been interpreted in terms of excitations to regions of high state density in the conduction band or in the band gap for the surface states. Heinrich *et al.*[53] reported EELS data on MgO(100) surfaces and interpreted the loss features in terms of transitions from the $2p$ and $2s$ states of Mg^{2+} to empty atomic orbitals of the dipositivie ion. One set of transitions was primarily surface sensitive, and the remaining transitions were bulk derived. The surface states were interpreted as arising from atomic transitions of the surface Mg^{2+} ions which were energy-shifted by a Stark field that was present at the surface of the ionic crystal. The energies of the bulk EELS transitions were in reasonable agreement with optical transitions for Mg^{2+} reported in Moore's tables.[54] However, the energy-level diagram of Fig. 12 shows that transitions to all but one of the various final states observed for sapphire occur from both O and Al initial states. This indicates that chemical bonding is important in the description of the final states of sapphire, in that they have both O and Al character, as shown by Ciraci and Batra in their band-structure calculation.[16] However, the regions of high state density in the sapphire band undoubtedly arise from atomiclike states of the ionic species in the crystal, modified by chemical bonding. The data of Henrich *et al.* may be used to construct a one-electron energy-level diagram similar to Fig. 12 using the XPS data by Kowalczyk *et al.*,[18,41] along with a 7.5-eV band gap derived from optical data.[55] The XPS data from Ref. 41 are summarized in Table I, and the conduction-band energy levels for MgO(100), which were derived by an analysis similar to that for sapphire, are shown in Table II. The most significant result is the surface state which lies 3.2 eV below the CBM of MgO. A slab calculation of the band structure of MgO(100) would be very useful in further analyzing the existing data sets for MgO.

E. XPS satellites

The most prominent XPS satellites, labeled *B*, *E*, and *L* in Figs. 2 and 3, occur about 25 eV below the O $2s$, Al $2p$, Al $2s$, and O $1s$ lines, respectively, and are undoubtedly due to energy loss from a photoelectron to a volume plasmon. Other strong features, labeled *G* and *M*, occur 50 eV below the Al $2s$ and O $1s$ lines and are due to double losses to the volume plasmon. The O $1s$ XPS data, in Fig. 3, also contain a slight rise, labeled *N*, which may be caused by a triple volume plasmon loss. An additional strong satellite of the O $1s$ photopeak, labeled *K* in Fig. 3, is seen at approximately 13 eV below the core line. Figure 10 shows that this XPS satellite has a corresponding EELS feature which has been identified as an interband transition.

The XPS data for the Al $2p$ and Al $2s$ energy levels also have satellites 13 eV below the core lines, labeled *A* and *D* in Fig. 2, which are due to the interband transition mentioned above. However, there are additional satellites labeled *F* and *H* through *J* in Fig. 2. A comparison of EELS and XPS data in Fig. 11 leads to the assignment of feature *F* as an Al $2s$ photoelectron which loses energy to an interband transition between the LVB and conduction band. A similar comparison for satellite *H* suggests that it may be due to losses from either an Al $2s$ photoelectron to an interband transition with an Al $2p$ initial state, or an Al $2p$ photoelectron exciting a transition with an Al $2s$ initial state. XPS satellites *I* and *J* could be due to similar processes, but the two XPS satellites correspond to only one EELS feature located at an energy intermediate to the two satellites. The absence of two features in this region of the EELS spectra may be due to the poor resolution of the CMA. The only completely unassigned satellite is the narrow peak labeled *C* in Fig. 2, which may be due to a shakeup process.

XPS data for many other metal oxides can be found throughout the literature.[41] The spectra of MgO and TiO_2 contain satellite peaks behind several of the core lines. These satellites are very similar to those observed in sapphire, which indicates that the loss peaks observed in these metal oxides are also caused by plasmon losses and interband transitions excited by the photoelectrons.

V. CONCLUSIONS

These investigations have demonstrated that the $(1\bar{1}02)$ surface of sapphire can be prepared so that it is extremely clean and well ordered. The surface has a 2×1 LEED pattern and does not trap appreciable amounts of charge during electron bombardment by either LEED or AES electron guns. However, when even submonolayer amounts of nickel are deposited on the surface, the sample charges up to as high as -350 V during electron bombardment.

An experimental, one-electron energy-level diagram has been constructed for sapphire from the data collected in this investigation and for MgO for literature data. The valence-band density of states of sapphire obtained from the XPS data, which has been corrected for cross-section effects, is in reasonable agreement with a band-structure calculation by Ciraci and Batra.[16] The regions of high electronic state density in the conduction band apparently arose from transitions to empty atomiclike orbitals of the constituent ions in the crystal. In addition, there is one empty surface state approximately 4 eV below the CBM of sapphire $(1\bar{1}02)$. This surface state reduces the effective band gap of the $(1\bar{1}02)$ sapphire surface from 8.5 to 4.5 eV. The state 1 eV below the CBM may be another surface state or an excitonic state. Finally, a series of satellites in the sapphire XPS data have been identified as energy losses to plasmons and interband transitions. XPS data for sapphire and other metal oxides have been in the literature for 10 years and the satellites have lacked a detailed explanation until now.

ACKNOWLEDGMENTS

This work was supported in part by the Universitywide Energy Research Group (UERG) of the University of California and by the Office of Naval Research. R.S.W. acknowledges the Camille and Henry Dreyfus Foundation and the Alfred P. Sloan Foundation for financial support. The authors thank I. Batra for his comments regarding this work and for supplying material encorporated into Figs. 1 and 12 of this paper.

*Present address: Hughes Research Laboratories, 3011 Malibu Canyon Rd., Malibu, CA 90265.
[1]G. H. C. Freeman, Brit. J. Appl. Phys. **16**, 927 (1965).
[2]G. Stephan, J. C. Lemonnier, and S. Robin, J. Opt. Soc. Am. **57**, 486 (1967).
[3]E. T. Arakawa and M. W. Williams, J. Phys. Chem. Solids **29**, 735 (1968).
[4]C. J. Powell and J. B. Swan, Phys. Rev. **118**, 640 (1960).
[5]N. Swanson, Phys. Rev. **165**, 1067 (1968).
[6]L. B. Leder, Phys. Rev. **103**, 1721 (1956).
[7]E. R. Il'mas and A. I. Kuznetsov, Fiz. Tverd. Tela (Leningrad) **14**, 1464 (1972) [Sov. Phys.—Solid State **14**, 1255 (1972)].
[8]E. Loh, Solid State Commun. **2**, 269 (1964).
[9]M. H. Reilly, J. Phys. Chem. Solids **31**, 1041 (1970).
[10]F. C. Douglas, Ph.D. thesis, University of Connecticut, 1970 (unpublished).
[11]J. A. Tossel, J. Am. Chem. Soc. **97**, 4840 (1975).
[12]J. A. Tossel, J. Phys. Chem. Solids **36**, 1273 (1975).
[13]K. L. Brower, J. Vac. Sci. Technol. **12**, 458 (1975).
[14]R. A. Evarestov, A. N. Ermoshkin, and V. A. Lovchikov, Phys. Status Solidi B **99**, 387 (1980).
[15]I. P. Batra, J. Phys. C **15**, 5399 (1982).
[16]S. Ciraci and I. P. Batra, Phys. Rev. B **28**, 982 (1983).
[17]A. Balzarotti and A. Bianconi, Phys. Status Solidi B **76**, 689 (1976).
[18]S. P. Kowalczyk, F. R. McFeely, L. Ley, V. T. Gritsyna, and D. A. Shirley, Solid State Commun. **23**, 161 (1977).
[19]K. Codling and R. P. Madden, Phys. Rev. **167**, 587 (1968).
[20]A. Balzarotti, A. Bianconi, E. Burattini, M. Grandolfo, R. Habel, and M. Piacentini, Phys. Status Solidi **63**, 77 (1974).
[21]A. Balzarotti, F. Antonangeli, R. Girlanda, and G. Martino, Phys. Rev. B **29**, 5903 (1984).
[22]A. Balzarotti, F. Antonangeli, R. Girlanda, and G. Martino, Solid State Commun. **44**, 275 (1982).
[23]V. A. Fomichev, Fiz. Tverd. Tela (Leningrad) **10**, 763 (1968) [Sov. Phys.—Solid State **8**, 2312 (1967)].
[24]I. A. Brytov and Y. N. Romashchenko, Fiz. Tverd. Tela (Leningrad) **20**, 2843 (1978) [Sov. Phys.—Solid State **20**, 384 (1978)].
[25]C. G. Dodd and G. L. Glen, J. Appl. Phys. **39**, 5377 (1968); J. Am. Ceram. Soc. **53**, 322 (1970).
[26]D. W. Fischer, Adv. X-Ray Anal. **13**, 159 (1970).
[27]C. Benndorf, G. Keller, H. Seidel, and F. Thieme, Surf. Sci. **67**, 589 (1977).
[28]J. Olivier and R. Poirier, Surf. Sci. **105**, 347 (1981).
[29]I. P. Batra and L. Kleinman, J. Electron Spectrosc. **33**, 175 (1984).
[30]A. Bianconi, R. Z. Bachrach, and S. A. Flodstrom, Phys. Rev. B **19**, 3879 (1979); Solid State Commun. **24**, 539 (1977).
[31]A. Bianconi, Surf. Sci. **89**, 41 (1979).
[32]α-Al_2O_3, also known as corundum, has rhombohedral symmetry. However, it is usually refered to hexagonal axes for simplicity. See, for example, R. W. G. Wyckoff, in *Crystal Structures II,* 2nd ed. (Wiley, New York, 1964), or R. Nolder and I. Cadoff, Trans. Metall. Soc. AIME **233**, 549 (1965).
[33]C. C. Chang, J. Appl. Phys. **39**, 5570 (1968).
[34]C. C. Chang, in *The Structure and Chemistry of Solid Surfaces,* edited by G. A. Somorjai (Wiley, New York, 1969), article 77-1.
[35]C. C. Chang, J. Vac. Sci. Technol. **8**, 500 (1971).
[36]J. C. Bean, Appl. Phys. Lett. **36**, 741 (1980).
[37]For a discussion of EELS theory and experiment, see H. Froitzheim, in *Electronic Spectroscopy for Surface Analysis,* edited by H. Ibach (Springer, Berlin, 1977), p. 205.
[38]J. E. Rowe and H. Ibach, Phys. Rev. Lett. **31**, 102 (1973).
[39]H. Ibach and J. E. Rowe, Phys. Rev. B **9**, 1951 (1974).
[40]J. H. Scofield, J. Electron. Spectrosc. **8**, 129 (1976).
[41]S. P. Kowalczyk, Ph.D. thesis, University of California, 1976 (unpublished).
[42]M. P. Seah and W. A. Dench, Surf. Interface Anal. **1**, 2 (1979).
[43]R. S. Williams, S. P. Kowalczyk, P. S. Wehner, G. Apai, J. Stöhr, and D. A. Shirley, J. Electron Spectrosc. Relat. Phenom. **12**, 477 (1977).
[44]H. Raether, in *Excitation of Plasmons and Interband Transitions by Electrons* (Springer, Berlin, 1980).
[45]B. D. Evans, H. D. Hendricks, F. D. Bazzarre, and J. M. Bunch, in *Ion Implantation in Semiconductors,* edited by F. Chernow, J. A. Borders, and D. K. Brice (Plenum, New York, 1977), p. 265.
[46]K. H. Lee and J. H. Crawford, Jr., Phys. Rev. B **19**, 3217 (1979).
[47]B. D. Evans and M. Stapelbroek, J. Nucl. Mater. **85-86**, 497 (1979).
[48]H. H. Tippins, Phys. Rev. B **1**, 126 (1970).
[49]P. W. Levy, Phys. Rev. **123**, 1226 (1961).
[50]E. W. J. Mitchell, J. D. Rigden, and P. D. Towsend, Philos. Mag. **5**, 1013 (1960).
[51]K. H. Lee and J. H. Crawford, Jr., Appl. Phys. Lett. **33**, 273 (1978).
[52]E. Harari and B. S. H. Royce, Appl. Phys. Lett. **22**, 106 (1973).
[53]V. E. Henrich, G. Dresselhaus, and H. J. Zeiger, Phys. Rev. Lett. **36**, 158 (1976).
[54]C. E. Moore, *Atomic Energy Levels,* U.S. National Bureau of Standards Circular No. 467 (U.S. GPO, Washington, D.C., 1949), Vol. 1.
[55]W. H. Strehlow and E. L. Cook, J. Phys. Chem. Ref. Data **2**, 163 (1973).